*Journal of Sound and Vibration* (1999) **219**(2), 339–357
*Article No*. jsvi.1998.1902, available online at http://www.idealibrary.com.on IDEAL

# NON-LINEAR VIBRATION OF A PIEZOELECTRIC BEAM CONTACTING WITH A FIXED DISK

R.-F. FUNG, J.-S. HUANG, D.-G. CHANG

*Department of Mechanical Engineering, Chung Yuan Christian University, Chung-Li, Taiwan* 32023, *Republic of China*

AND

C.-M. YAO

*National Center for High-Performance Computing, Hsinchu, Taiwan, Republic of China*

(*Received* 26 *May* 1997, *and in final form* 3 *August* 1998)

Non-linear vibrations of a cantilever piezoelectric beam in contact with a fixed disk are studied in this paper. The piezoelectric beam is excited to produce mechanical longitudinal oscillations by inverse piezoelectric effect of piezoceramics. The equations of motion describing the vibrations and contact forces are derived by Hamilton's principle and the geometry constraint. Finite element formulation is used to reduce the equations to a set of non-linear ordinary differential equations. The transient amplitudes and the contacting forces are simulated by the Runge–Kutta algorithm. The effects of piezoceramics, excitation of voltage and the frictional forces are investigated and discussed.



## 1. INTRODUCTION

In recent years, piezomotors have been increasingly discussed as a superior alternative to electromagnetic motors in special areas of application. A conventional ultrasonic motor consists of a stator and a disk. The stator is ultrasonically excited by piezoelectric materials and this piezoelectrically stimulated mechanical oscillation is used to drive the disk via friction forces [1]. Because of their coupled mechanical and electrical properties [2–4], piezoceramics have recently attracted significant attention for their potential application as sensors for monitoring and as actuators for controlling the response of structures. An increasing amplitude of motion at the end of the resonator was achieved by suitably tapering the resonator and through this a motor was built up for one direction of rotation with an efficiency of around 35% [5].

Although many authors have obtained some impressive results for ultrasonic motors, they have not derived the mathematical model explicitly. Generally, the piezoelectric characterization is a difficult problem. Numerous investigators [6]

0022–460X/99/020339 + 19 $30.00/0 

have recently demonstrated the practicability of the integrated concept through the use of simple structures such as cantilever beams. Several analysis and numerical models [7, 8] have also been developed to analyze the integrated structures. Most of the numerical models were based on simplified structures under simple loading conditions. Although finite element methods have been developed for piezoelectric structures, the use of finite element techniques for analyzing the integrated piezo-composite structures has not been fully established [9, 10].

In this paper, the results of the forced vibrations of a cantilever beam in contact with a fixed disk are studied. The piezoelectric beam is excited by inverse piezoelectric effect. The configuration of the test structure is shown in Figure 1. It is composed of a piece PZT G1195N and a steel beam. The formulation is based on the general concept of constitutive law in piezoelectric materials [11–13]. Applying the geometry constraint at the contact point and the Lagrange multiplier method, the interaction forces enforce the constraint conditions between the

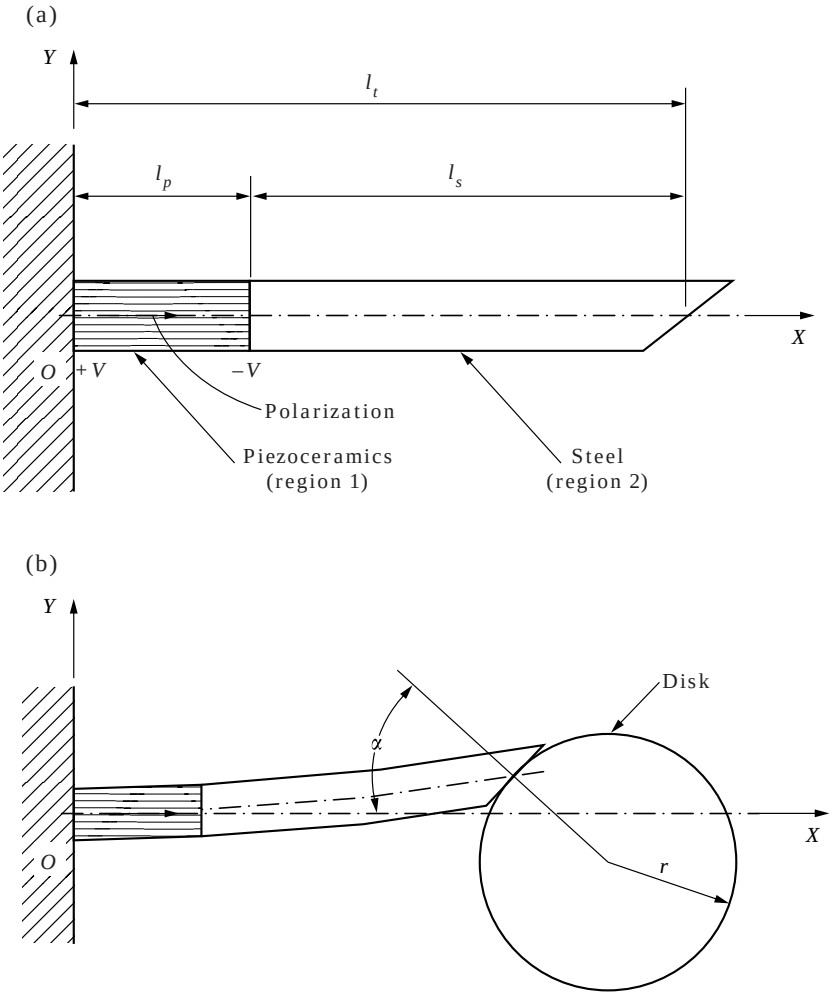


Figure 1. Schematic diagram of the piezoelectric beam (a) and the disk (b).

piezoelectric beam and the fixed disk. Hamilton's principle and calculus of variation are employed to derive the governing equations. Finally, the assembly governing equations are solved by use of the Runge–Kutta integration numerical method. The model developed enables one to investigate the behavior of the non-linear vibration in transient responses.

## 2. FORMULATIONS OF THE PHYSICAL MODEL

### 2.1. MODEL

The model including a piezoelectric beam and a fixed disk is shown in Figure 1. Region 1 of the beam of piezoceramics having length $l_p$, while region 2 is steel having length $l_s$, both having thickness $h$ and width $b$. The cantilever beam consists of the piezoceramics and steel having total length $l_t$. The beam is pressed to a fixed disk with radius $R$ and with an angle $\alpha$ with respect to its normal. It is demanded that the beam is initially pressed to the disk by a normal force $N_0$. Figure 2 shows the initial and the operating states of the piezoelectric beam. In Figure 3 we have the displacement relationship with $u_{N_e+1}$ and $v_{N_e+1}$ at end point $B$. The beam is modelled as a Timoshenko beam and Hamilton's principle is used to derive the equations of motion of the system.

The direct and inverse piezoelectric phenomena consist of an interaction between the mechanical and the electrical behaviors of a material. The constitutive equations [14] of the piezoceramics can be expressed as

$$T_{ij} = c^E_{ijkl} S_{kl} - e_{kij} E_k, \qquad D_i = e_{ikl} S_{kl} + \varepsilon^S_{ik} E_k, \tag{1, 2}$$

where $T_{ij}$, $S_{kl}$, $E_k$ and $D_i$ are stress, strain, electric field and electric displacement components, respectively, $c^E_{ijkl}$ are the elastic coefficients at a constant electric field strength, $e_{ijk}$ are the piezoelectric coefficients and $\varepsilon^S_{ik}$ are the dielectric coefficients at a constant elastic stress.

The strain–displacement relations for small deformations can be written as

$$S_{ij} = \tfrac{1}{2}(u_{i,j} + u_{j,i}), \tag{3}$$

and the electric fields $E_k$ are related to the electric potential $\phi$ by

$$E_k = -\phi_{,k}. \tag{4}$$

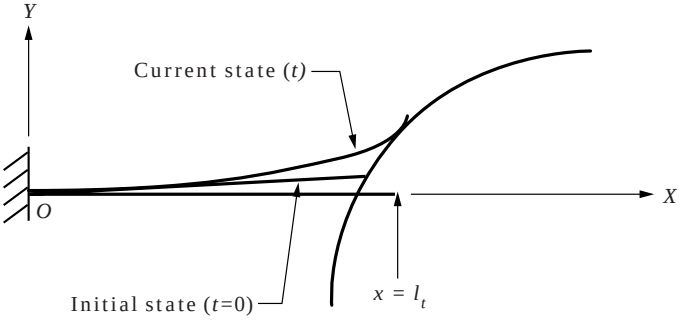


Figure 2. The initial and the operating states of the piezoelectric beam.

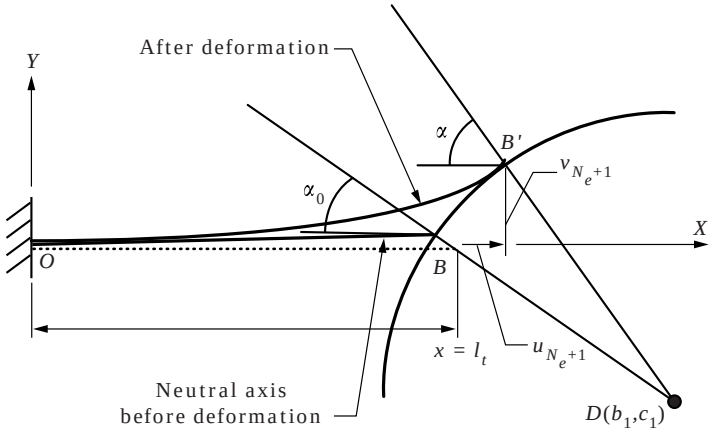


Figure 3. The displacement relationship between $u_{N_e+1}$ and $v_{N_e+1}$ at end point $B$.

## 2.2. FINITE ELEMENT FORMULATION

The technique of the finite element method was developed by many authors to analyze the devices fabricated from piezoelectric materials [9, 10, 15]. The formulation procedure is similar to the standard one for structure mechanics described in reference [16].

Two co-ordinate systems $OXY$ and $o'xy$ are shown in Figure 4. **i** and **j** are unit vectors of the global coordinate system $OXY$ while $\mathbf{e}_i$ and $\mathbf{e}_j$ are unit vectors of the local element co-ordinate system $o'xy$.

The displacement field of the Timoshenko beam is

$$u_1(x, t) = u(x, t) - y\psi(x, t), \qquad u_2(x, t) = v(x, t) \tag{5}$$

where $u$ and $v$ represent the axial and transverse displacements of the piezoelectric beam, respectively, and $\psi$ is the rotating angle of the cross-section.

The position vector of an arbitrary point $P_i$ in the $i$th element with respect to the global co-ordinate system is

$$\mathbf{R}(x, y, t) = (R_0 + x + u - y\psi)\mathbf{i} + (y + v)\mathbf{j}, \tag{6}$$

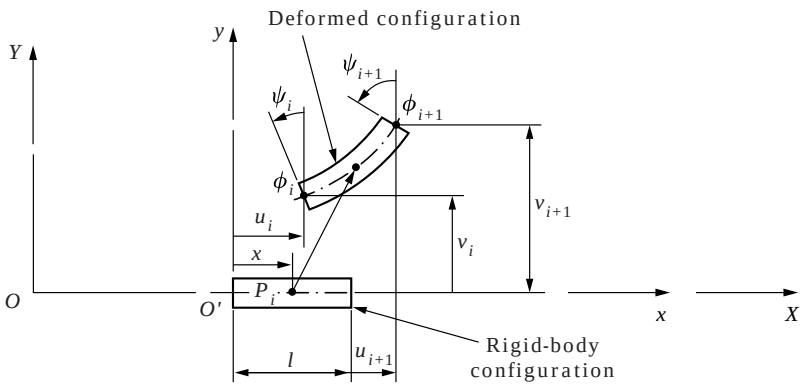


Figure 4. The $i$th beam element undergoing gross motion and elastic deformation.

where $R_0$ is the distance from the origin $O$ of the global co-ordinate to the origin $o'$ of the local co-ordinate. The distance $R_0$ of each element in regions 1 and 2 are respectively

$$R_0 = \begin{cases} \dfrac{(i-1)}{m} l_p, & i = 1, 2, \ldots, m; \\ l_p + \dfrac{(i-1)}{n} l_s, & i = 1, 2, \ldots, n, \end{cases} \tag{7}$$

where $m$ and $n$ are the numbers of elements in the piezoceramics and the steel, respectively.

By differentiating equation (6) with respect to time $t$, the absolute velocity vector is

$$\mathbf{R}_t(x, y, t) = (u_t - y\psi_t)\mathbf{i} + v_t\mathbf{j}. \tag{8}$$

The kinetic energy of the piezoelectric beam can be expressed as

$$T = \frac{1}{2}\int_V \rho \mathbf{R}_t(x, y, t) \cdot \mathbf{R}_t(x, y, t)\, \mathrm{d}V. \tag{9}$$

where $\rho$ is the mass density and $V$ is the volume of the beam.

The linear Lagrangian strains are

$$S_{11} = u_x - y\psi_x, \qquad S_{22} = 0, \qquad S_{12} = S_{21} = \tfrac{1}{2}(v_x - \psi), \tag{10}$$

and the electric field is

$$E_1 = -\phi_x. \tag{11}$$

The total potential energy for region 1 of the piezoceramics can be expressed as [12]

$$U_1 = \frac{1}{2}\int_V (\{S\}^T[c^E]\{S\} - \{S\}^T[e]\{E\} - \{E\}^T[e]^T\{S\} - \{E\}^T[\varepsilon^S]\{E\})\, \mathrm{d}V, \tag{12a}$$

and for region 2 of the steel is

$$U_2 = \frac{1}{2}\int_V \{S\}^T[c^E]\{S\}\, \mathrm{d}V. \tag{12b}$$

The mechanical and electrical works are respectively

$$W_F = \mathbf{F}_F \cdot \mathbf{R}(l_t, 0, t), \qquad W_Q = -\int_A \phi\{v_\phi\}^T\{D\}\, \mathrm{d}A, \tag{13, 14}$$

where $\mathbf{F}_F$ is the external contact force applied at $x = l_t$, $\phi$ is the electric potential and $\{v_\phi\}$ is the vector of surface direction cosines. Figure 5 shows the interaction

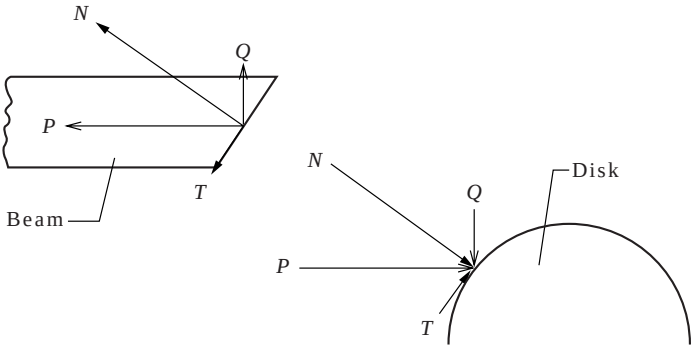


Figure 5. The piezoelectric beam and rotor in the regime of slip.

forces for the piezoelectric beam and disk in the regime of slip. The virtual work done by the current contact force $\mathbf{F}_F$ on the piezoelectric beam at $x = l_t$ is

$$\delta W_F = \mathbf{F}_F \cdot \delta\mathbf{R}(l_t, 0, t) = -P\delta u(l_t, t) + Q\delta v(l_t, t), \tag{15}$$

where the following relations are used

$$\mathbf{F}_F = -P\mathbf{i} + Q\mathbf{j}, \qquad \delta\mathbf{R}(l_t, 0, t) = \delta u(l_t, t)\mathbf{i} + \delta v(l_t, t)\mathbf{j}. \tag{16, 17}$$

The forces of $P$ and $Q$ are the axial compressive force and the transverse force, respectively.

The usual approach of the finite element method is to assume each unknown deformation to be approximated by a finite series of polynomials [17]. The deflection $v$ and angle $\psi$ of the beam element can be described by using the cubic polynomials as

$$v = a_0 + a_1 x + a_2 x^2 + a_3 x^3, \qquad \psi = b_0 + b_1 x + b_2 x^2 + b_3 x^3,$$

and the deflection $u$ and electric potential $\phi$ of the beam element by using the polynomials as

$$u = c_0 + c_1 x, \qquad \phi = d_0 + d_1 x,$$

where $a_0 \sim a_3$, $b_0 \sim b_3$, $c_0 \sim c_1$ and $d_0 \sim d_1$ are coefficients to be determined.

For each element the non-dimensional parameter $\xi = x/l$ is used, where $l$ is the length of an element. It is noted that the piezoceramics and the steel have different element lengths. The element deflections $u$, $v$ and $\psi$, and electrical potential $\phi$ are approximated as follows:

$$\begin{Bmatrix} u \\ v \\ \psi \end{Bmatrix} = \begin{bmatrix} N_{u1} & 0 & 0 & N_{u2} & 0 & 0 \\ 0 & N_{v1} & N_{v2} & 0 & N_{v3} & N_{v4} \\ 0 & N_{\psi 1} & N_{\psi 2} & 0 & N_{\psi 3} & N_{\psi 4} \end{bmatrix} \begin{Bmatrix} u_i \\ v_i \\ \psi_i \\ u_{i+1} \\ v_{i+1} \\ \psi_{i+1} \end{Bmatrix} = \mathbf{N}_u \mathbf{q}_u, \tag{18}$$

$$\phi = [N_{\phi 1} \quad N_{\phi 2}] \begin{Bmatrix} \phi_i \\ \phi_{i+1} \end{Bmatrix} = \mathbf{N}_\phi \mathbf{q}, \tag{19}$$

where $\mathbf{q}_u = [u_i \ v_i \ \psi_i \ u_{i+1} \ v_{i+1} \ \psi_{i+1}]^T$ is the nodal displacement vector and $\mathbf{q}_\phi = [\phi_i \ \phi_{i+1}]^T$ is the nodal electric potential vector for the $i$th element, and $N_{u1}, N_{u2}, \ldots N_{v3}, N_{v4}, \ldots, N_{\psi 3}, N_{\psi 4}, N_{\phi 1}, N_{\phi 2}$ are polynomial shape functions. Details of the shape functions are given in Appendix A.

The derivatives of $u$, $v$, $\psi$ and $\phi$ with respect to $x$ within the $i$th element can be written, respectively, as

$$u_x = \frac{\mathrm{d}u}{\mathrm{d}x} = [B_u]\mathbf{q}_u, \qquad v_x = \frac{\mathrm{d}v}{\mathrm{d}x} = [B_v]\mathbf{q}_u, \tag{20a, b}$$

$$\psi_x = \frac{\mathrm{d}\psi}{\mathrm{d}x} = [B_\psi]\mathbf{q}_u, \qquad \phi_x = \frac{\mathrm{d}\phi}{\mathrm{d}x} = [B_\phi]\mathbf{q}_\phi, \tag{20c, d}$$

where

$$[B_u] = \frac{\mathrm{d}}{\mathrm{d}x}[N_u], \qquad [B_v] = \frac{\mathrm{d}}{\mathrm{d}x}[N_v], \qquad [B_\psi] = \frac{\mathrm{d}}{\mathrm{d}x}[N_\psi], \qquad [B] = \frac{\mathrm{d}}{\mathrm{d}x}[N_\phi].$$

Substituting equations (20a–d) into equations (9) and (12a–b), we have the kinetic and potential energies of an element as

$$T_e = \tfrac{1}{2}\dot{\mathbf{q}}_u^T[m]\dot{\mathbf{q}}_u, \tag{21}$$

$$U_{1e} = \tfrac{1}{2}(\mathbf{q}_u^T[k_{uu}]\mathbf{q}_u + \mathbf{q}_u^T[k_{u\phi}]\mathbf{q}_\phi + \mathbf{q}_\phi^T[k_{\phi u}]\mathbf{q}_u - \mathbf{q}_\phi^T[k_{\phi\phi}]\mathbf{q}_\phi), \tag{22a}$$

$$U_{2e} = \tfrac{1}{2}\mathbf{q}_u^T[k_{uu}]\mathbf{q}_u, \tag{22b}$$

where $[m]$, $[k_{uu}]$, $[k_{u\phi}]$, $[k_{\phi u}]$ and $[k_{\phi\phi}]$ can be seen in Appendix B.

The displacements at each nodal point of the beam element are assumed to be composed of the axial deformation $u$, transverse deformation $v$ and angle $\psi$. For the piezoceramics beam element, each node has an additional degree of freedom of electric potential $\phi$. Then each node for the piezoceramics has four degrees of freedom $u$, $v$, $\psi$ and $\phi$.

### 2.3. GEOMETRIC CONSTRAINT AND HAMILTON'S PRINCIPLE

The geometric constraint will be investigated at the end point where the beam is in contact with the disk. In Figure 3, point $D$ at position $(b_1, c_1)$ is the center of the fixed disk, point $B$ is the end point of the beam before deformation. The position vector after deformation at point $B'$ is

$$\mathbf{R}_{OB'} = \mathbf{R}^f(l_t, 0, t) = (l_t + u_{N_e+1})\mathbf{i} + v_{N_e+1}\mathbf{j}, \tag{23}$$

where $N_e$ is the total number of elements of the beam.

From the triangle $\Delta OB'D$, one has the relationship

$$\mathbf{R}_{OD} - \mathbf{R}_{OB'} = \mathbf{R}_{B'D}. \tag{24}$$

Thus, the geometric constraint condition can be written as

$$C = (l_t + u_{N_e+1} - b_1)^2 + (v_{N_e+1} - c_1)^2 - r^2 = 0. \tag{25}$$

Hamilton's principle used without considering the constraint equation (25) is

$$\int_{t_1}^{t_2} \left( \sum_{i=1}^{N_e} \delta L_i + \delta W_F + \delta W_Q \right) \mathrm{d}t = 0, \tag{26}$$

where the Lagrangian function of each element is $L_i = T_i - U_i$. Performing the variation on the Lagrangian function of each element, one obtains

$$\begin{aligned} \int_{t_1}^{t_2} \sum_{i=1}^{N_e} \delta L_i \, \mathrm{d}t = \int_{t_1}^{t_2} \Bigg[ \sum_{i=1}^{m} \left( \delta \mathbf{q}_{ui}^T \left( \frac{\partial L_i}{\partial \mathbf{q}_{ui}} - \frac{\mathrm{d}}{\mathrm{d}t} \frac{\partial L_i}{\partial \dot{\mathbf{q}}_{ui}} \right) + \delta \mathbf{q}_{\phi i}^T \left( \frac{\partial L_i}{\partial \mathbf{q}_{\phi i}} - \frac{\mathrm{d}}{\mathrm{d}t} \frac{\partial L_i}{\partial \dot{\mathbf{q}}_{\phi i}} \right) \right) \\ + \sum_{j=1}^{n} \delta \mathbf{q}_{uj}^T \left( \frac{\partial L_j}{\partial \mathbf{q}_{uj}} - \frac{\mathrm{d}}{\mathrm{d}t} \frac{\partial L_j}{\partial \dot{\mathbf{q}}_{uj}} \right) \Bigg] \mathrm{d}t \\ + \left[ \sum_{i=1}^{m} \left( \delta \mathbf{q}_{ui}^T \frac{\partial L_i}{\partial \dot{\mathbf{q}}_{ui}} + \delta \mathbf{q}_{\phi i}^T \frac{\partial L_i}{\partial \dot{\mathbf{q}}_{\phi i}} \right) + \sum_{j=1}^{n} \delta \mathbf{q}_{uj}^T \frac{\partial L_j}{\partial \dot{\mathbf{q}}_{uj}} \right]_{t_1}^{t_2}, \end{aligned} \tag{27}$$

The varied path concides with the true path at the two end times $t_1$ and $t_2$. It follows that $\delta \mathbf{q}_u(t_1) = \delta \mathbf{q}_u(t_2) = 0$ and $\delta \mathbf{q}_\phi(t_1) = \delta \mathbf{q}_\phi(t_2) = 0$.

After substituting equations (13), (14), (21), (22) and (24) into equation (23), and since point $O$ is fixed and the corresponding nodal displacements $u_1$, $v_1$ and $\psi_1$ are specified by the boundary conditions $u_1 = v_1 = \psi_1 = 0$, i.e., $\delta u_1 = \delta v_1 = \delta \psi_1 = 0$, the global ordinary differential equation of the system can be obtained as

$$\begin{bmatrix} \mathbf{M}_{uu} & 0 \\ 0 & 0 \end{bmatrix} \begin{Bmatrix} \ddot{\mathbf{Q}}_u \\ \ddot{\mathbf{Q}}_\phi \end{Bmatrix} + \begin{bmatrix} \mathbf{K}_{uu} & \mathbf{K}_{u\phi} \\ \mathbf{K}_{u\phi}^T & -\mathbf{K}_{\phi\phi} \end{bmatrix} \begin{Bmatrix} \mathbf{Q}_u \\ \mathbf{Q}_\phi \end{Bmatrix} = \begin{Bmatrix} \mathbf{F}_F \\ \mathbf{F}_Q \end{Bmatrix}, \tag{28}$$

where $\mathbf{Q}_u = \{u_2, v_2, \psi_2, \ldots, u_{N_e+1}, v_{N_e+1}, \psi_{N_e+1}\}^T$ is the nodal displacement vector, $\mathbf{Q}_\phi = \{\phi_1, \ldots, \phi_{m+1}\}^T$ is the electric potential vector, $\mathbf{M}_{uu}$ is the mass matrix, $\mathbf{K}_{uu}$, $\mathbf{K}_{u\phi}$ and $\mathbf{K}_{\phi\phi}$ are the mechanical, piezoelectric and dielectric stiffness matrices, respectively. $\mathbf{F}_F$ is the mechanical force vector and $\mathbf{F}_Q$ is the electrical charge vector.

The equations of initial condition can be determined from equation (28) by neglecting the time-dependent terms and the piezoelectric effects. Thus, one has

$$\mathbf{Q}_u = \mathbf{K}_{uu}^{-1} \cdot \mathbf{F}_F, \tag{29}$$

where

$$\mathbf{F}_F = [0, 0, 0, \ldots, -P_0, Q_0, 0]^T, \tag{30}$$

$P_0$ and $Q_0$ are the initial pressed forces in the longitudinal and transverse directions, respectively. $P_0$ and $Q_0$ are decomposed directly from $N_0$.

### 2.4. REDUCTION OF SYSTEM EQUATIONS

Equation (28) describes the dynamic behavior of a cantilever piezoelectric beam. As the piezoelectric beam is excited by an applied voltage across two electrodes on the left and right surfaces of the piezoceramics, these two equipotential surfaces

have the difference of electrical potentials. Therefore, the electrical boundary conditions at the right surface of the electrode is usually grounded, and the electrical potential on the grounded electrode $\phi_r$ is set to zero. Moreover, the left surface of ungrounded electrodes has an electrical potential $\phi$ then the $\mathbf{F}_{Q_p}$ is the nodal charge on the left ungrounded electrode surface. The electrical potential vector of the system can be set as [15]

$$Q_\phi = \begin{Bmatrix} Q_{\phi_r} \\ Q_{\phi_i} \\ Q_{\phi_p} \end{Bmatrix}. \tag{31}$$

Then equation (28) can be partitioned as

$$\begin{bmatrix} \mathbf{M}_{uu} & 0 & 0 \\ 0 & 0 & 0 \\ 0 & 0 & 0 \end{bmatrix} \begin{Bmatrix} \ddot{\mathbf{Q}}_u \\ \ddot{\mathbf{Q}}_{\phi_i} \\ \ddot{\mathbf{Q}}_{\phi_p} \end{Bmatrix} + \begin{bmatrix} \mathbf{K}_{uu} & \mathbf{K}_{u\phi_i} & \mathbf{K}_{u\phi_p} \\ \mathbf{K}_{u\phi_i}^T & -\mathbf{K}_{\phi_i\phi_i} & -\mathbf{K}_{\phi_i\phi_p} \\ \mathbf{K}_{u\phi_p}^T & -\mathbf{K}_{\phi_i\phi_p}^T & -\mathbf{K}_{\phi_p\phi_p} \end{bmatrix} \begin{Bmatrix} \mathbf{Q}_u \\ \mathbf{Q}_{\phi_i} \\ \mathbf{Q}_{\phi_p} \end{Bmatrix} = \begin{Bmatrix} \mathbf{F}_F \\ 0 \\ \mathbf{F}_{Q_p} \end{Bmatrix}, \tag{32}$$

where the subscripts $i$ and $p$ denote the non-electrode nodes which include the internal nodes and the ungrounded electrode nodes, respectively. Identically, $\mathbf{Q}_{\phi_i}$ is the electrical potential vector corresponding to the non-electrode nodes, and $\mathbf{Q}_{\phi_p}$ is the electrical potential vector corresponding to the nodes on the ungrounded electrode surface.

The first two sets of equation (32) can be rewritten as

$$\begin{bmatrix} \mathbf{M}_{uu} & 0 \\ 0 & 0 \end{bmatrix} \begin{Bmatrix} \ddot{\mathbf{Q}}_u \\ \ddot{\mathbf{Q}}_{\phi_i} \end{Bmatrix} + \begin{bmatrix} \mathbf{K}_{uu} & \mathbf{K}_{u\phi_i} \\ \mathbf{K}_{u\phi_i}^T & -\mathbf{K}_{\phi_i\phi_i} \end{bmatrix} \begin{Bmatrix} \mathbf{Q}_u \\ \mathbf{Q}_{\phi_i} \end{Bmatrix} = \begin{Bmatrix} \mathbf{F}_F - \mathbf{K}_{u\phi_p}\mathbf{Q}_{\phi_p} \\ \mathbf{K}_{\phi_i\phi_p}\mathbf{Q}_{\phi_p} \end{Bmatrix}. \tag{33}$$

If $\mathbf{Q}_{\phi_p}$ is specified as an input for the actuator, the second set of equations in equation (33) can be used to relate $Q_{\phi_i}$ in terms of $Q_{\phi_p}$. Then the first set of equation (33) can be rewritten as

$$\mathbf{M}_{uu}\ddot{\mathbf{Q}}_u + \mathbf{K}'_{uu}\mathbf{Q}_u = \mathbf{F}_F - \mathbf{F}_\phi, \tag{34}$$

where

$$\mathbf{K}'_{uu} = \mathbf{K}_{uu} + \mathbf{K}_{u\phi_i}\mathbf{K}_{\phi_i\phi_i}^{-1}\mathbf{K}_{u\phi_i}^T, \tag{35}$$

$$\mathbf{F}_\phi = (\mathbf{K}_{u\phi_p} - \mathbf{K}_{u\phi_i}\mathbf{K}_{\phi_i\phi_i}^{-1}\mathbf{K}_{\phi_i\phi_p})\mathbf{Q}_{\phi_p}, \tag{36}$$

and $\mathbf{F}_\phi$ is defined as the electrical force vector produced by the specified voltage vector at the piezoceramics.

## 3. FRICTIONAL CONTACT

In order to demonstrate the accuracy of the developed algorithms, the frictional contact between the piezoelectric beam and fixed disk is involved. Furthermore, this study accounts for the effect of deformation of the piezoelectric beam upon the resulting contact forces. The most common methods of treating the geometrical contact problems are based on the Lagrange multiplier. As it is

employed, the geometric condition is enforced by augmenting the Lagrange multiplier as the additional system variables.

Sequentially, the external contact force vector $\mathbf{F}_F$ is calculated by means of two terms [18]. The first one is the product of the scalar Lagrange multiplier with the gradient of the constraint, and represents the generalized normal reaction force $\lambda \cdot \mathbf{B}^T$. The second represents the generalized friction force $|\lambda| \cdot \mathbf{Q}_f$, where $|\lambda|$ is replaced by $\lambda$ sign $(\lambda)$. The constraint matrix is

$$\mathbf{B} = \left[0, 0, 0, \ldots, \frac{\partial C}{\partial u_{N_e+1}}, \frac{\partial C}{\partial v_{N_e+1}}, 0\right],$$

and the friction force vector is

$$\mathbf{Q}_f = \mu\left\{0, 0, 0, \ldots, \frac{-\partial C}{\partial v_{N_e+1}}, \frac{\partial C}{\partial u_{N_e+1}}, 0\right\},$$

where $\mu$ is the coefficient of dry friction.

The constraint matrix $\mathbf{B}$ contains coefficients which are functions of the geometry of contact; therefore, $\mathbf{B}$ is an implicit function of time and can be differentiated with respect to time as follows:

$$\dot{C} = \mathbf{B}\dot{\mathbf{Q}}_u = 0, \qquad \ddot{C} = \dot{\mathbf{B}}\dot{\mathbf{Q}}_u + \mathbf{B}\ddot{\mathbf{Q}}_u = 0. \tag{37, 38}$$

To simulate the motion of the piezoelectric beam in contact with the fixed disk, equations (34) and (38) should be solved together.

Equation (34) is premultiplied by $\mathbf{M}_{uu}^{-1}$ and rearranged as follows:

$$\ddot{\mathbf{Q}}_u = \mathbf{M}_{uu}^{-1}[-\mathbf{K}'_{uu}\mathbf{Q}_u + \mathbf{F}_F - \mathbf{F}_\phi], \tag{39}$$

where $\mathbf{F}_F = \lambda(\mathbf{B}^T + \text{sign}\,(\lambda)\mathbf{Q}_f)$.

Combining equations (38) and (39), the Lagrange multiplier is obtained as:

$$\lambda = [\mathbf{B}\mathbf{M}_{uu}^{-1}(\mathbf{B}^T + \text{sign}\,(\lambda)\mathbf{Q}_f)]^{-1} \cdot [-\mathbf{B}\mathbf{Q}_u + \mathbf{B}\mathbf{M}_{uu}^{-1}(\mathbf{K}\mathbf{Q}_u + \mathbf{F}_\phi)]. \tag{40}$$

Equations (39) and (40) are the foundations for a numerical procedure solution of the equations of motion (34) and the constraint (25). The procedure as described above is repeated at each time point in the numerical simulation. Initial conditions which satisfy the constraint conditions (25) and its condition of time derivative (37) are selected.

## 4. TREATING GEOMETRIC CONSTRAINT

In order to improve the numerical accuracy for this constrained dynamics system, direct treatment of the geometric constraint is used. From equation (25) $u_{N_e+1}$ and $v_{N_e+1}$ are related by

$$v_{N_e+1} = \sqrt{r^2 - (l_t + u_{N_e+1} - b_1)^2} + c_1. \tag{41a}$$

TABLE 1

*The material properties of piezoceramics and steel*

| | Piezoceramic | Steel |
|---|---|---|
| Young's modulus (GPa): $E$ | 63·0 | 220 |
| Poisson's ratio: $v$ | 0·3 | 0·3 |
| Shear modulus (GPa): $G$ | 24·2 | 84·6 |
| Density (kg/m$^3$): $\rho$ | 7600 | 7800 |
| Piezoelectric (C/m$^2$): | | |
| $e_{111}$ | 16·002 | 0 |
| $e_{112}$ | 36·792 | 0 |
| Dielectric (nN/V$^2$): $\varepsilon_{11}^S$ | 15·3 | 0 |

The velocity and acceleration are, respectively,

$$\dot{v}_{N_e+1} = -\frac{l_t + u_{N_e+1} - b_1}{\sqrt{r^2 - (l_t + u_{N_e+1} - b_1)^2}}\,\dot{u}_{N_e+1}, \tag{41b}$$

$$\ddot{v}_{N_e+1} = -\frac{(l_t + u_{N_e+1} - b_1)\ddot{u}_{N_e+1} + \dfrac{r^2\dot{u}_{N_e+1}^2}{r^2 - (l_t + u_{N_e+1} - b_1)^2}}{\sqrt{r^2 - (l_t + u_{N_e+1} - b_1)^2}}. \tag{41c}$$

By substituting equation (41) into equation (34), and eliminating the $(3N_e + 2)$th row and column of equation (34), the equation can be solved by the numerical method. Once $v_{N_e+1}$ is obtained, the longitudinal displacement

$$u_{N_e+1} = \pm\sqrt{r^2 - (v_{N_e+1} - c_1)^2} + b_1 - l_t$$

can be determined, where the negative sign is taken for the compressed beam.

It is known that the angle $\alpha$ depends on time. In Figure 3, the two vectors $OB'$ and $DB'$ are respectively

$$OB' = (l_t + u_{N_e+1})\mathbf{i} + (v_{N_e+1})\mathbf{j}, \tag{42}$$

TABLE 2

*Comparison of natural frequencies* (Hz) *for the cantilever beam*

| Mode | Free vibration (steel) | Free vibration (piezo + steel) | Boundary constraint (piezo + steel) |
|---|---|---|---|
| $v$(I) | 3521·72 | 2625·04 | 12 736·81 |
| $v$(II) | 21 310·63 | 18 454·16 | 39 461·89 |
| $v$(III) | 60 739·06 | 51 558·10 | 85 682·11 |
| $v$(IV) | 107 404·20 | 97 179·51 | 132 713·66 |
| $v$(V) | 191 609·88 | 148 882·25 | 145 823·94 |
| $u$(I) | 57 466·04 | 49 863·59 | 44 937·08 |
| $u$(II) | 207 926·83 | 162 555·79 | 228 044·84 |

$v$(I): first bending mode, $v$(II): second bending mode, $v$(III): third bending mode, $v$(IV): fourth bending mode, $v$(V): fifth bending mode, $u$(I): first axial mode, $u$(II): second axial mode.

$$DB' = (l_t + u_{N_e+1} - b_1)\mathbf{i} + (v_{N_e+1} - c_1)\mathbf{j}. \tag{43}$$

Using the inner product one obtains the angle $\alpha$ as

$$\alpha = \pi - \cos^{-1}\left(\frac{(l_t + u_{N_e+1})(l_t + u_{N_e+1} - b_1) + v_{N_e+1}(v_{N_e+1} - c_1)}{\sqrt{(l_t + u_{N_e+1})^2 + v_{N_e+1}^2}\sqrt{(l_t + u_{N_e+1} - b_1)^2 + (v_{N_e+1} - c_1)^2}}\right). \tag{44}$$

## 5. NUMERICAL RESULTS AND DISCUSSION

Dimensions of the piezoelectric beam are the length of piezoceramics $l_p = 2$ mm and the length of steel $l_s = 20$ mm. The piezoceramic beam is assumed to be uniform with width $b = 5$ mm and thickness $h = 2$ mm. The material properties of piezoceramics and steel are listed in Table 1. The disk is made of steel, which is assumed to be rigid compared with the flexible beam, with thickness 2·5 mm and radius $r = 20$ mm. The coefficient of dry friction $\mu$ and shape factor $K$ of the Timoshenko beam are taken to be 0·2 and 0·85, respectively. The initially normal force pressed to the piezoelectric beam is $N_0 = 9{\cdot}81$ N and the initial angle $\alpha_0 = 30^\circ$, so the initial longitudinal and transverse displacements of the piezoelectric beam $u_0(x)$ and $v_0(x)$ can be determined from the static analysis of equation (29).

In order to study the non-linear vibrations of the piezoelectric beam, the finite element technique is used to solve this problem. The Runge–Kutta integration scheme is utilized to simulate the system dynamics. Six elements, including two

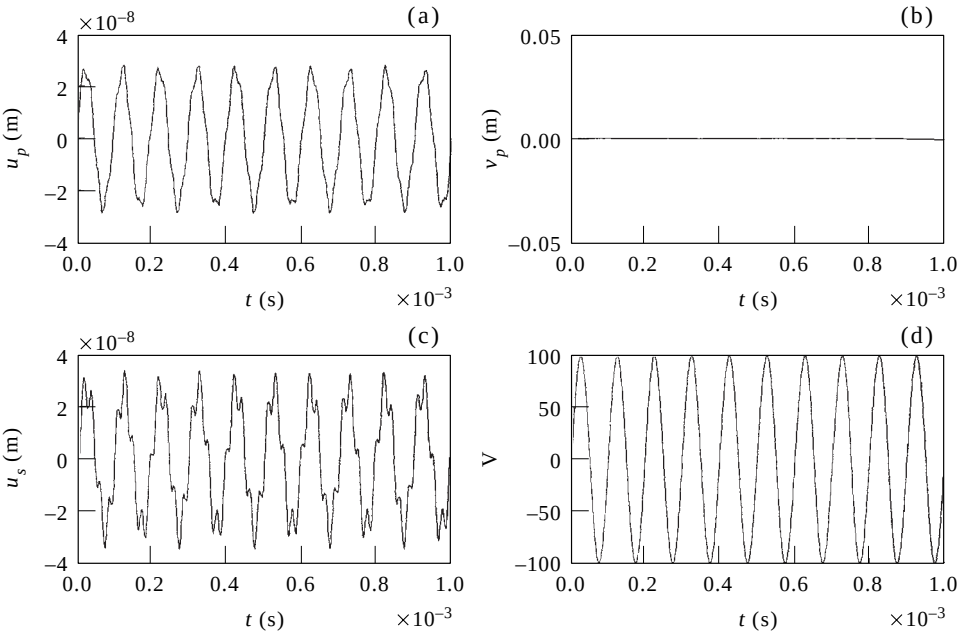


Figure 6. The axial and transverse transient amplitudes of the piezoelectric beam for the free vibration. (a) The transient axial deflection $u_p$ at $x = l_p$. (b) The transient transverse deflection $v_p$ at $x = l_p$. (c) The transient axial deflection $u_s$ at $x = l_t$. (d) The external voltage.

elements in the piezoceramics and four elements in the steel, are taken to analyze the piezoelectric beam. Good accuracy is achieved by comparing with the higher numbers of elements (not shown here). Table 2 gives the comparison of frequencies of the longitudinal and transverse modes for both free vibrations and boundary constraint. For free vibration, we can find that the frequencies for piezoceramics and steel are smaller than those for only steel. This is because Young's modulus

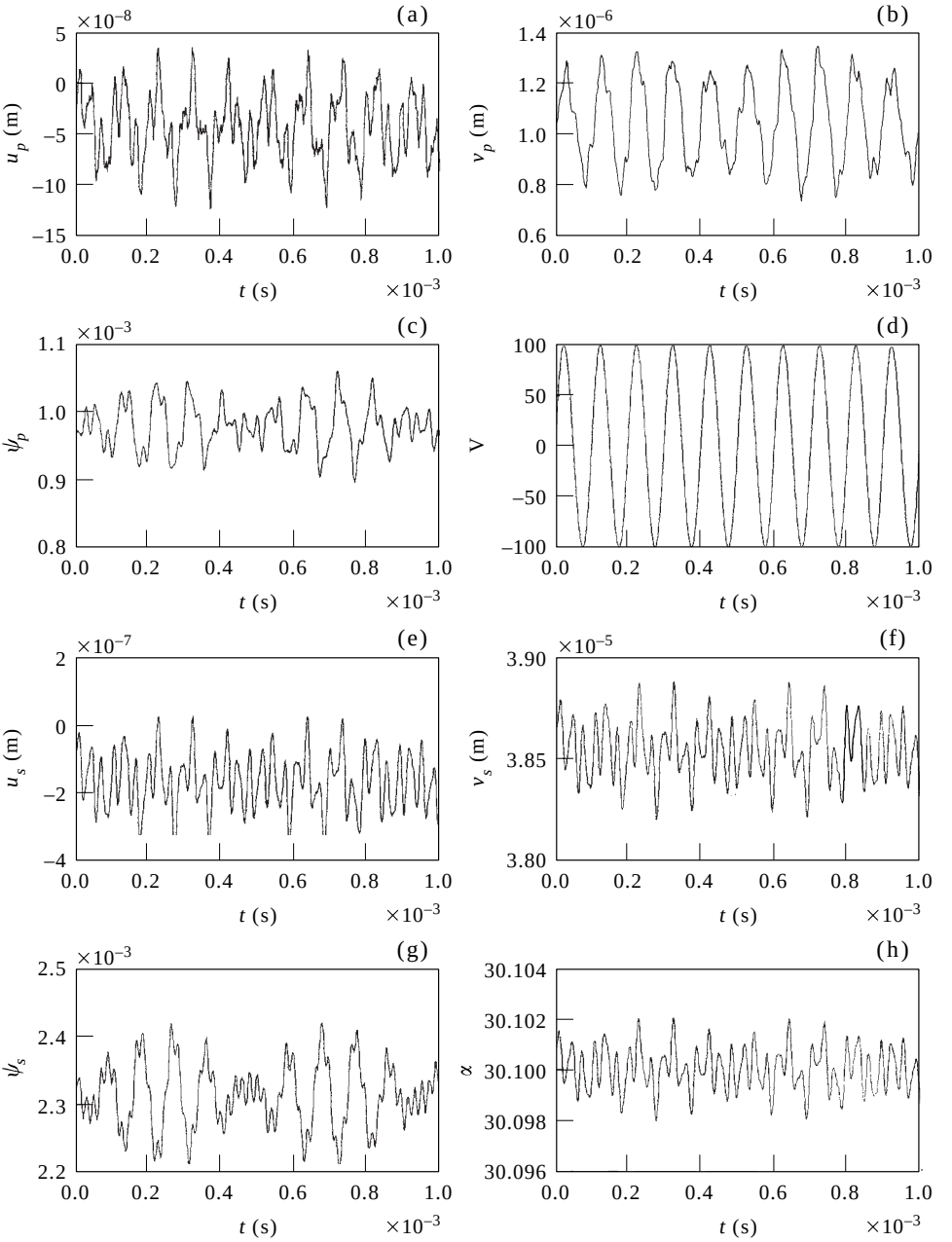


Figure 7(a–h)—(*Caption on following page*).

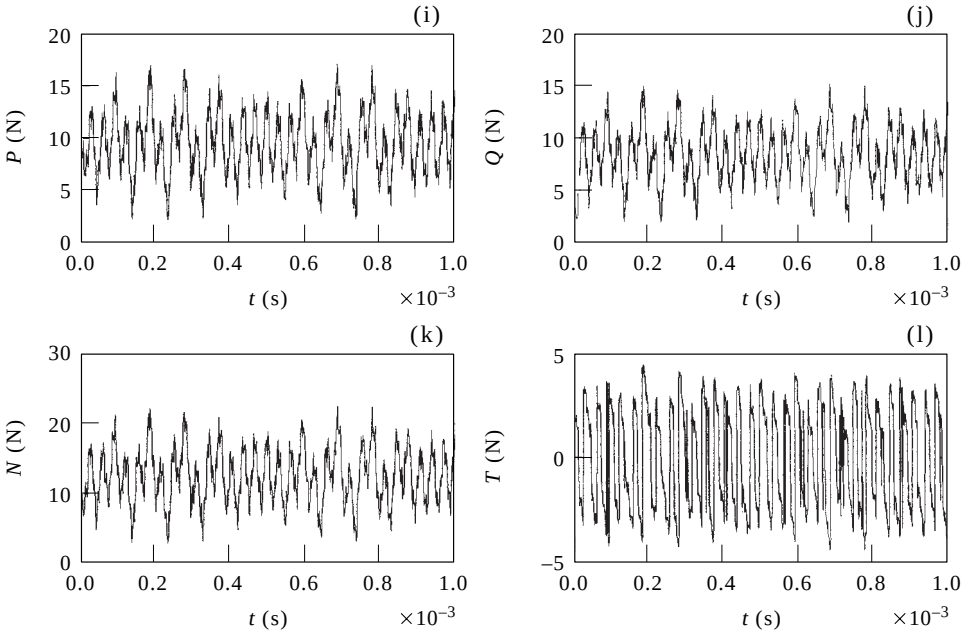


Figure 7(i–l)

Figure 7. The transient amplitudes and contacting forces for the piezoelectric beam for the forced vibration. (a) The transient axial deflection $u_p$ at $x = l_p$. (b) The transient transverse deflection $v_p$ at $x = l_p$. (c) The transient slop $\psi_p$ at $x = l_p$. (d) The external voltage. (e) The transient axial deflection $u_s$ at $x = l_t$. (f) The transient transverse deflection $v_s$ at $x = l_t$. (g) The transient slope $\psi_s$ at $x = l_t$. (h) Time history of angle $\alpha$. (i) Time history of axial force $P$. (j) Time history of transverse force $Q$. (k) Time history of normal force $N$. (l) Time history of frictional force $T$.

of the piezoceramics is smaller than that of steel. For the boundary constraint case, the frequencies are much higher. When the external excitation of voltage is close to one of the constrained frequency, the system can obtain a most effective response.

For free vibration the geometric constraint is absent, and $\lambda = 0$. Figure 6 shows the transient response of the piezoceramics due to a 10 kHz sine input on the actuator with 100 V amplitude. Figures 6(a) and (c) show the transient amplitudes for the axial deflection at $x = l_p$ and $x = l_t$, respectively. From Figure 6(a), it is observed that the motion of this point is not a sine function as voltage input, due to the coupling dynamics between piezoceramics and steel. Thus, the assumption of pure sinusoidal motion used to drive the steel beam as in reference [1] may introduce errors even in this simple free vibration case. More noisy shapes at beam tip can be seen in Figure 6(c). Figure 6(b) shows the transverse displacement at $x = l_p$ is zero, because the voltage is not applied in the transverse direction. The periodic sinusoidal voltage applied in the axial direction is shown in Figure 6(d).

For the forced constrained vibrations, the geometric constraint is investigated and the interactions of frictional forces are included. Figures 7(a)–(c) show the transient responses of the piezoelectric beam at $x = l_p$, due to a 10 kHz sine input on the piezoceramics with 100 V amplitude. Figure 7(d) shows the periodic sinusoidal voltage applied in the axial direction. Because of the contact behavior,

Figure 7(a) shows that the shape is more noisy and is quite different from the sine function. Thus, the simple sinusoidal motion assumed in reference [1] will yield unsatisfactory results. Figures 7(e)–(g) show the transient responses of the piezoelectric beam at $x = l_t$. Figure 7(h) shows the variation of angle $\alpha$ with time. It is seen that the magnitude of variation of the angle is quite small compared with

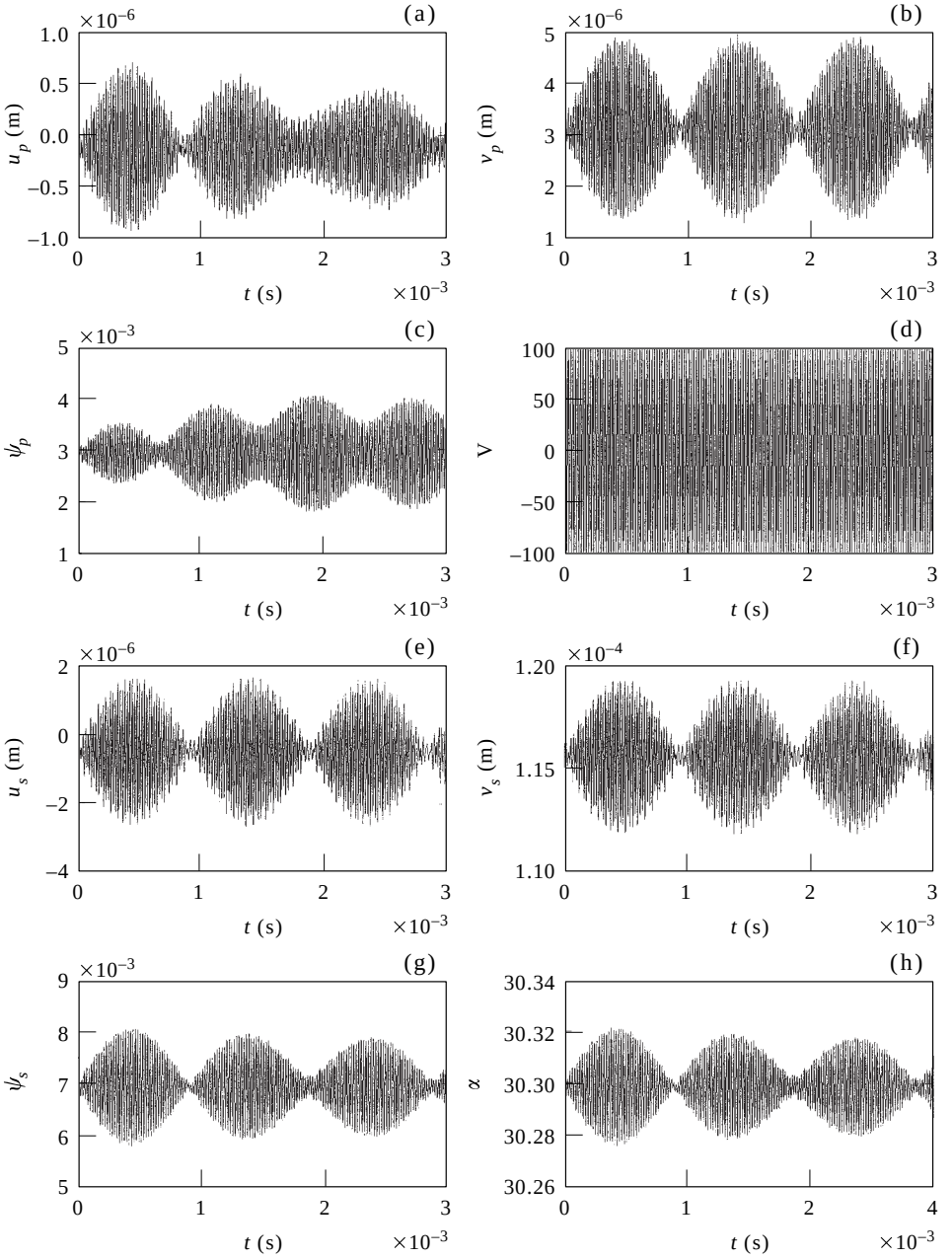


Figure 8(a–h)—(*Caption on following page*).

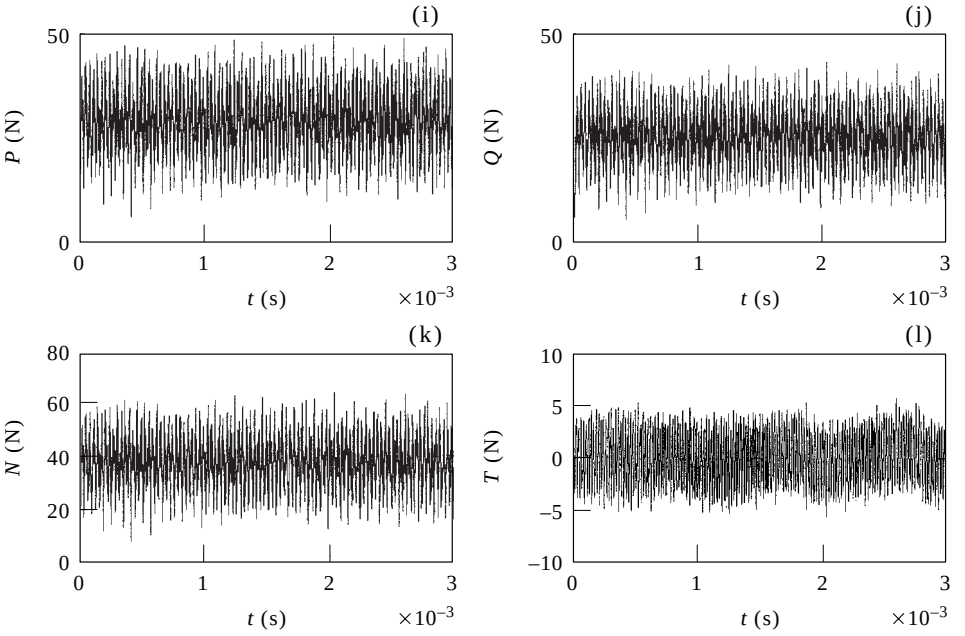


Figure 8(i–l)

Figure 8. The transient responses of the piezoelectric beam for the beating phenomena. (a) The transient axial deflection $u_p$ at $x = l_p$. (b) The transient transverse deflection $v_p$ at $x = l_p$. (c) The transient slop $\psi_p$ at $x = l_p$. (d) The external voltage. (e) The transient axial deflection $u_s$ at $x = l_t$. (f) The transient transverse deflection $v_s$ at $x = l_t$. (g) The transient slope $\psi_s$ at $x = l_t$. (h) Time history of angle $\alpha$. (i) Time history of axial force $P$. (j) Time history of transverse force $Q$. (k) Time history of normal force $N$. (l) Time history of frictional force $T$.

$\alpha_0$. Figures 7(i)–(l) show the interaction forces at the contact point. These directions of the interaction forces are decided from Figure 5.

If the system is subjected to harmonic excitation and its excitation frequency is equal to its natural frequency, resonance will occur and the transient amplitude increases infinitely. If the applied voltage frequency is close to, but not exactly equal to the natural frequency of the system, a phenomenon known as beating may occur. Figures 8(a)–(l) show the beating phenomenon of the transient amplitudes and the contacting forces of the system under $N_0 = 29{\cdot}43$ N and 50 000 Hz voltage frequency which is close to the natural frequency 44 937 Hz in Table 2. This beating phenomenon can also be seen in Figures 7(a)–(l), since the 10 kHz voltage frequency is also close to the natural frequency 12 737 Hz in Table 2.

## 6. CONCLUSIONS

The behavior of non-linear vibrations of a piezoelectric beam in contact with a fixed disk is studied in this paper. These formulations are based on the general concept of constitutive law in piezoelectric materials and Hamilton's principle allowing the introduction of kinetic energy, electrical energy, and geometric constraints relating the deformation variables. Then, the equations are solved by

using the Runge–Kutta integration numerical method, and the vibration responses of the piezoelectric beam are investigated with the sinusoidal input voltage.

From the results, we can draw the following conclusions: (1) The simple assumption of sinusoidal motion of the piezoelectric material used in analysis of piezomotor may introduce large errors. Thus, in the design and analysis of piezomotor, a full model consisting of the coupling behavior of piezoelectricity and structure should be considered. (2) In dealing with the constrained motion, a procedure has been presented for incorporating dry friction force into the model, which is based on the state variables and the magnitude of contacting force. The analysis procedure developed here could be easily extended to treat the more complex and realistic model of piezomotors.

## ACKNOWLEDGMENT

Support of this work by the National Center for High-Performance Computing of the Republic of China under Contract NCHC-86-05-013 is gratefully acknowledged.

## REFERENCES

1. O. Y. Zharil 1993 *Institute of Electrical and Electronic Engineers*, *Transactions on Ultrasonics Ferroelectrics and Frequency Control* **40**, 411–416. Modeling of a mode conversion ultrasonic motor in the regime of slip.
2. H. F. Tiersten and R. D. Mindlin 1962 *Quarterly Journal of Applied Mathematics* **20**, 107. Forced vibrations of piezoelectric crystal plates.
3. J. Zelenka 1986 *Piezoelectric Resonators and Their Applications*. New York.
4. B. A. Auld 1990 *Acoustic Fields and Waves in Solids*. Melbourne, FL.
5. M. Fleisher, D. Stein and H. Meixner 1989 *Institute of Electrical and Electronic Engineers*, *Transactions on Ultrasonics Ferroelectrics and Frequency Control* **36**, 607–613. Ultrasonic piezomotor with longitudinally oscillating amplitude-transforming resonator.
6. T. B. Bailey and J. E. Hubbard 1985 *Journal of Guidance Control and Dynamics* **8**, 605–611. Distributed piezoelectric-polymer active vibration control of a cantilever beam.
7. N. W. Hagood, W. H. Chung and A. V. Flotow 1990 *Proceedings of the AIAA/ASME/ASCE/AHS/ASC* 31*st Structures*, *Structural Dynamics and Materials Conference*, *American Institute of Aeronautics and Astronautics Journal New York*, 2242–2256. Modeling of piezoelectric actuator dynamics for active structural control.
8. S. Im and S. N. Atluri 1989 *American Institute of Aeronautics and Astronautics Journal* **27**, 1801–1807. Effects of a piezo-actuator on a finitely deformed beam subject to general loading.
9. H. Allik and T. J. R. Hughes 1970 *International Journal for Numerical Methods in Engineering* **2**, 151–157. Finite element method for piezoelectric vibration.
10. M. Naillon, R. Coursant and F. Besnier 1983 *Acta Electronica* **25**, 341–362. Analysis of piezoelectric structures by a finite element method.
11. M. Fleischer, D. Stein and H. Meixner 1990 *Sensors and Actuators* **A21–A23**, 357–361. Novel ultrasonic motors with mono- and bimodal drives.
12. M. A. Moetakef, K. L. Lawrence, S. P. Joshi and P. S. Shiakolas 1995 *American Institute of Aeronautics and Astronautics Journal* **33**, 136–142. Closed-form expressions for higher order electroelastic tetrahedral elements.

13. K. J. BATHE 1982 *Finite Element Procedures in Engineering Analysis*. Englewood Cliffs, NJ: Prentice-Hall.
14. S. K. HA, C. KEILERS and F. K. CHANG 1992 *American Institute of Aeronautics and Astronautics Journal* **30**, 772–780. Finite element analysis of composite structures containing distributed piezoceramic sensors and actuators.
15. N. GUO and P. CAWLEY 1992 *Journal of Sound and Vibration* **159**, 115–138. The finite element analysis of the vibration characteristics of piezoelectric discs.
16. O. C. ZIENKIEWICZ 1971 *The Finite Element Method in Engineering Science*. New York: McGraw-Hill.
17. B. M. BAHGAT and K. D. WILLMERT 1976 *Mechanism and Machine Theory* **11**, 47–71. Finite element vibrational analysis of planar mechanisms.
18. C. W. GEAR, B. LEIMKUHLER and G. K. GUPTA 1985 *Journal of Computational and Applied Mathematics* **12/13**, 77–90. Automatic integration of Euler–Lagrange equations with constraints.

## APPENDIX A

Details of the shape functions of equations (18, 19) are:

$$N_{u1} = 1 - \xi, \qquad N_{u2} = 1 - \xi, \qquad N_{\phi 1} = 1 - \xi, \qquad N_{\phi 2} = \xi,$$

$$N_{v1} = \frac{1 - 3\xi^2 + 2\xi^3 + (1 - \xi)\eta}{1 + \eta}, \qquad N_{v2} = \frac{[\xi - 2\xi^2 + \xi^3 + (\xi - \xi^2)\eta/2]l}{1 + \eta},$$

$$N_{v3} = \frac{3\xi^2 - 2\xi^3 + \xi\eta}{1 + \eta}, \qquad N_{v4} = \frac{[-\xi^2 + \xi^3 - (\xi - \xi^2)\eta/2]l}{1 + \eta},$$

$$N_{\psi 1} = \frac{6(-\xi + \xi^2)}{l(1 + \eta)}, \qquad N_{\psi 2} = \frac{1 - 4\xi + 3\xi^2 + (1 - \xi)\eta}{1 + \eta},$$

$$N_{\psi 3} = \frac{6(\xi - \xi^2)}{l(1 + \eta)}, \qquad N_{\psi 4} = \frac{-2\xi + 3\xi^2 + \xi\eta}{1 + \eta},$$

where $\eta = 12EI/KGAl^2$.

## APPENDIX B

For the kinetic energy (21) and the potential energy (22a, 22b) of an element:

$$[m] = \int_0^l \{\rho A\{[N_u]^T[N_u] + [N_v]^T[N_v]\} + \rho I[N_\psi]^T[N_\psi]\}\,\mathrm{d}x,$$

$$[k_1] = \int_0^l EA[B_u]^T[B_u]\,\mathrm{d}x,$$

$$[k_2] = \int_0^l EI[B_\psi]^T[B_\psi]\,\mathrm{d}x,$$

$$[k_3] = \int_0^l KGA\{[B_v]^T[B_v] - [B_v]^T[N_\psi] - [N_\psi]^T[B_v] + [N_\psi]^T[N_\psi]\}\,\mathrm{d}x,$$

$$[k_{uu}] = [k_1] + [k_2] + [k_3],$$

$$[k_{u\phi}] = [k_{\phi u}]^T = \int_0^l A\{e_{11}\{[B_u]^T[B_\phi]\} + e_{12}\{[B_v]^T[B_\phi] - [N_\psi]^T[B_\phi]\}\}\,\mathrm{d}x,$$

$$[k_{\phi\phi}] = \int_0^l \varepsilon_{11} A\{[B_\phi]^T[B_\phi]\}\,\mathrm{d}x.$$